Title

Does the Traditional Band Picture Correctly Describe the Electronic Structure of n-Doped Conjugated Polymers? A TD-DFT and Natural Transition Orbital Study.

Journal

Journal of Chemical Theory and Computation, 20(22)

Authors

Wu, Eric
Schwartz, Benjamin

Publication Date

2024-11-26

DOI

10.1021/acs.jctc.4c00817

Peer reviewed

JCTC Journal of Chemical Theory and Computation

pubs.acs.org/JCTC Article

Does the Traditional Band Picture Correctly Describe the Electronic Structure of n-Doped Conjugated Polymers? A TD-DFT and Natural Transition Orbital Study

Published as part of Journal of Chemical Theory and Computation special issue "First-Principles Simulations of Molecular Optoelectronic Materials: Elementary Excitations and Spatiotemporal Dynamics".

Eric C. Wu* and Benjamin J. Schwartz*

Cite This: J. Chem. Theory Comput. 2024, 20, 10059−10070 Read Online

ABSTRACT: Doped conjugated polymers have a variety of potential applications in thermoelectric and other electronic devices, but the nature of their electronic structure is still not well understood. In this work, we use time-dependent density functional theory (TD-DFT) calculations along with natural transition orbital (NTO) analysis to understand electronic structures of both p-type (e.g., poly(3-hexylthiophene-2,5-diyl), P3HT) and n-type (e.g., poly{[*N*,*N*′-bis(2-octyldodecyl)-naphthalene-1,4,5,8-bis(dicarboximide)-2,6-diyl]-*alt*-5,5′-(2,2′-bithiophene)}, N2200) conjugated polymers that are both p-doped and n-doped. Of course, the electronic transitions of doped conjugated polymers are multiconfigurational in nature, but it is still useful to have a one-electron energy level diagram with which to interpret their spectroscopy and other electronic behaviors. Based on the NTOs associated with the TD-DFT transitions, we find that the "best" one-electron orbital-based energy level diagram for doped conjugated polymers such as P3HT is the so-called traditional band picture. We also find that the situation is more complicated for donor−acceptor-type polymers like N2200, where the use of different exchange-correlation functionals leads to different predicted optical transitions that have significantly less one-electron character. For some functionals, we still find that the "best" one-electron energy level diagram agrees with the traditional picture, but for others, there is no obvious route to reducing the multiconfigurational transitions to a one-electron energy level diagram. We also see that the presence of both electron-rich and electron-poor subunits on N2200 breaks the symmetry between n- and p-doping, because different types of polarons reside on different subunits leading to different degrees of charge delocalization. This effect is exaggerated by the presence of dopant counterions, which interact differently with n- and p-polarons. Despite these complications, we argue that the traditional band picture suffices if one wishes to employ a simple one-electron picture to explain the spectroscopy of n- and p-doped conjugated polymers.

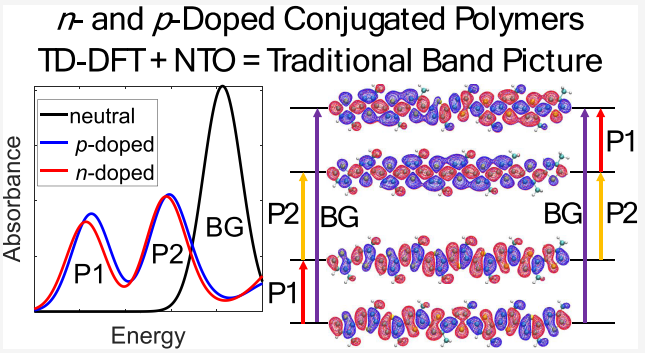

I. INTRODUCTION

Organic semiconducting conjugated polymers typically have low conductivities due to low intrinsic charge carrier densities. To increase the density of charge carriers, semiconducting polymers can be oxidized (p-doped) or reduced (n-doped) to introduce holes or electrons, respectively, onto the conjugated polymer backbone. The addition of new charge carriers changes the electronic structure of the doped polymer relative to the pristine material. Although the electronic structure of doped inorganic semiconductors is well understood, there is still not a consensus on the nature of the electronic energy levels of doped conjugated polymers. Currently, the literature uses two different one-electron models for the electronic structure of doped polymers: the traditional band picture,[1−9] which borrows from the language of inorganic semiconductors, and a density-functional-theory projected-density-of-states-based (DFT PDOS-based) model that has sometimes been referred to as the "band-bending" picture.[10−13] The two models are summarized in Figure 1a,b.

When an electron is removed from the highest occupied molecular orbital (HOMO) level of the conjugated π-system of the polymer backbone in p-doping, several repeat units of the

Received: June 23, 2024
Revised: October 25, 2024
Accepted: November 4, 2024
Published: November 14, 2024

https://doi.org/10.1021/acs.jctc.4c00817
J. Chem. Theory Comput. 2024, 20, 10059−10070

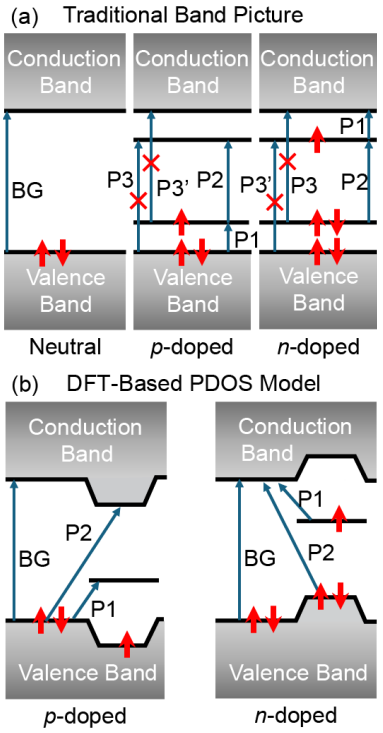

Figure 1. (a) Energy level diagrams for p- and n-doped conjugated polymers in the traditional band picture, where both n- and p-doping cause two states to move into the gap, inducing new optical transitions labeled P1 and P2. The energies of the transitions are similar for both types of doping. For p-doping, the ending orbital of the P1 transition is the same as the starting orbital of the P2 transition, while for n-doping, the starting orbital of the P1 transition is the same as the ending orbital of the P2 transition. (b) Energy level diagrams for p- and n-doped polymers in a model based on the projected density of states from DFT calculations, where the conduction and valence bands bend up or down for n- and p-doping, respectively, and only one state moves into the gap. The starting orbitals of the P1 and P2 transitions are the same for p-doping, while the ending orbitals of the P1 and P2 transitions are the same for n-doping.

polymer change structure from aromatic to quinoidal. The quinoidally distorted segment, along with both the charge and the unpaired spin, are together referred to as a polaron. In the traditional band picture, this reorganization of the polymer backbone causes two energy states move into the bandgap (BG), where the lower intragap state is half-filled and the upper intragap state is empty (Figure 1a). This, in turn, creates two symmetry-allowed optical transitions, labeled P1 and P2 ("P" for polaron) in order of their energy. For n-doping, an electron added to the conduction band creates a mirror-image situation that also causes a quinoidal distortion and pushes two states into the gap, where the lower state is filled and the upper state is half-filled. This also creates symmetry-allowed P1 and P2 optical transitions.

For both p- and n-doping, the symmetry of band-folding demands that the two states move into the gap by the same amount of energy. Therefore, for both types of doping, the P1 and P2 transitions should occur at roughly the same energies, and the following relation should hold:

$$E_{BG} \approx 2 \times E_{P1} + E_{P2} \quad (1)$$

where E_{BG}, E_{P1}, and E_{P2} are the energies of the BG, P1, and P2 transitions, respectively.

The traditional band picture is supported by ultrafast transient absorption experiments.[14−17] For p-doped materials, the traditional picture predicts that photoexciting the P1 transition transfers an electron from the valence band (i.e., an undoped polymer segment) to fill the hole (lower intragap state). This should then lead to a bleach of the P1 and bandgap (BG) transitions, as well as an induced absorption of the P2 transition, which is exactly what has been observed for multiple conjugated polymers with different dopants.[14−17] We note that the predicted transient spectroscopy for n-doped materials should be different: the removal of the electron from the upper intragap state by exciting the P1 transition should increase the P2 absorption by unblocking the upper state, but there should be no accompanying bleach of the BG transition. Although Wen et al.[18] and Gish et al.[19] performed ultrafast transient absorption experiments on the undoped n-type polymer poly{[*N*,*N*′-bis(2-octyldodecyl)-naphthalene-1,4,5,8-bis(dicarboximide)-2,6-diyl]-*alt*-5,5′-(2,2′-bithiophene)} (N2200, for chemical structure see Figure 2c), to the best of our knowledge, ultrafast transient absorption experiments have yet to be performed on any n-doped semiconducting polymers.

In addition to the P1 and P2 transitions, the traditional picture for both p- and n-doped semiconducting polymers predicts the existence of two symmetry-forbidden transitions, P3 and P3′, which are indicated by red X's in Figure 1a. On the basis of quantum chemistry calculations, Brédas and co-workers explained that these transitions can become partially allowed when there is disorder among the polymer chains or when there is some degree of delocalization of polarons between the π-stacks of neighboring polymer chains.[3,20] We and others have seen evidence for the presence of a partially allowed P3 transition both in steady-state absorption spectroscopy[21−24] and in ultrafast transient absorption experiments on p-doped conjugated polymers.[14,17]

Although the traditional band picture is generally widely accepted, Heimel[10] and others[11,12] have proposed a new model based on the projected density of states (PDOS) from DFT calculations. In this model, which is summarized in Figure 1b, instead of two states moving symmetrically into the gap upon doping, the aromatic-to-quinoidal structure change causes the valence and conduction bands to bend and only one unfilled state moves into the gap. For p-doping, both the valence and conduction bands bend downward, and the unpaired electron occupies the bent valence band region; the picture is symmetric for n-doping but with upward bending.

A major difference between the DFT-based PDOS model and the traditional band picture is the description of what happens when there are multiple charges on a single chain. The DFT-based PDOS model predicts that the lowest energy state is a triplet bipolaron,[10−12] whereas the traditional band picture predicts a spinless bipolaron. We showed previously that whether two polarons spin-pair to form a spinless bipolaron or simply *J*-couple depends on the positions of the counterions.[25] We also identified the spectroscopic signatures of polarons, coupled polarons, and bipolarons at different doping levels using both chemical and electrochemical doping.[25]

Another significant difference between the PDOS and the traditional band picture is that for p-doping in the PDOS picture, the P1 and P2 transitions start at the same state. This implies that photoexcitation of P1 should bleach the P1, P2, and BG transitions, which is contrary to what is observed in ultrafast transient absorption experiments.[14−17] Another difference between the traditional band picture and the DFT-based

https://doi.org/10.1021/acs.jctc.4c00817
J. Chem. Theory Comput. 2024, 20, 10059−10070

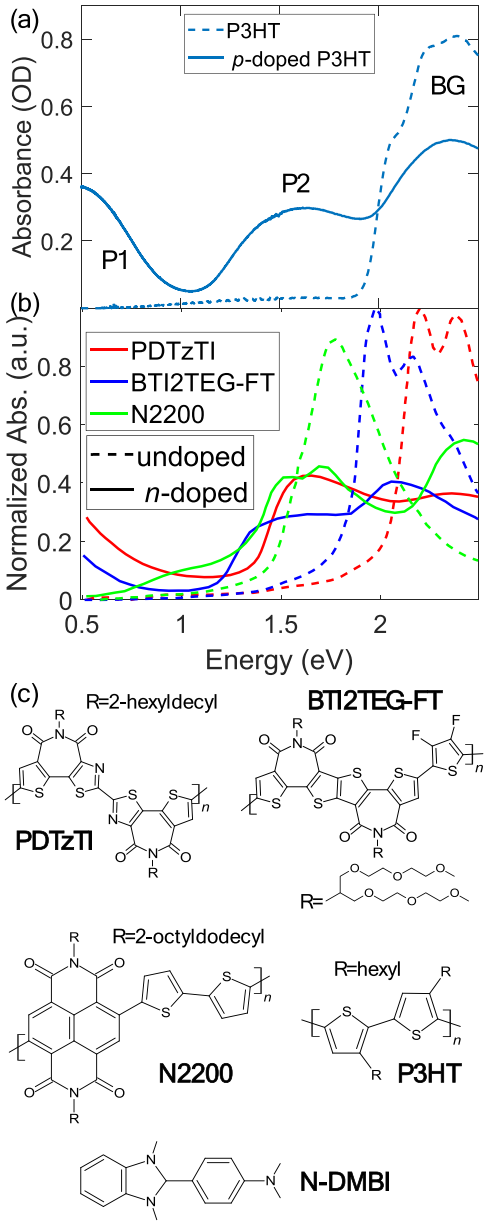

Figure 2. UV−vis−NIR absorption spectra of pristine (solid curves) and doped (dashed curves) (a) p-type and (b) n-type polymers. The P3HT films in (a) were cast from a 20 mg mL^{-1} solution of P3HT in *o*-dichlorobenzene. The doped film was created using sequential processing[38−42] with a 1 mM solution of $FeCl_3$ in *n*-butylacetate. The normalized absorption spectra of the pristine and doped n-type polymers in (b) were reproduced from ref 31. The films were doped with (4-(2,3-dihydro-1,3-dimethyl-1*H*-benzimidazol-2-yl)-*N*,*N*-dimethylbenzenamine) (N-DMBI), a commonly used dopant for n-type polymers. (c) Chemical structures of the n-type semiconducting polymers PDTzTI, BTI2TEG-FT, and N2200, the p-type semiconducting polymer P3HT, and N-DMBI.

PDOS model is that there are no P3 and P3′ transitions in the DFT-based PDOS model, even though these have been experimentally observed.[3,14,17,20−24,26]

All of this leads to the question of how to reconcile the PDOS model from DFT calculations with ultrafast transient absorption experiments[14−17] and the observation of P3 transitions. Recently, we showed that TD-DFT calculations were able to reproduce the experimental UV−vis−NIR spectrum (Figure 2a) of doped p-type poly(3-hexylthiophene-2,5-diyl) (P3HT; see Figure 2c for chemical structure).[27] Because the optical transitions in TD-DFT calculations have multiconfigurational character, we used natural transition orbital (NTO) analysis to provide the best possible one-electron picture to compare with the electronic structure diagrams in Figure 1. We found that the combination of TD-DFT, the use of a hybrid functional, the inclusion of counterions, and NTO analysis led to a one-electron orbital-based energy level diagram where the ending orbital for the P1 transition is the same as the starting orbital for the P2 transition; the calculations also predicted the presence of P3 and P3′ transitions with low oscillator strengths. Moreover, when the shift of the vacuum level is accounted for (by aligning the energy levels using TD-DFT calculated excited states and NTO analysis), the calculations were also able to show that the polaron is harder to oxidize than the neutral polymer. Thus, although there is no perfect one-electron diagram describing the electronic structure of doped polymers, these calculations indicated that the most accurate simple representation for p-doped P3HT is the traditional band picture.

The calculations described above, however, were only performed on a single p-type doped conjugated polymer. In general, there are relatively few experimental and computational studies of n-type polymers.[18,19,28−37] Although both the traditional and DFT-based PDOS models predict a partial bleach of the BG transition and the induced presence of P1 and P2 transitions upon both n- and p-doping, these features are not always observed experimentally in doped n-type polymers. Figure 2b shows that for some n-doped conjugated polymers, there are clear signatures of doping-induced P1 and P2 transitions at 0.5 and 1.5 eV,[31] similar to that of p-doped P3HT in Figure 2a. However, for n-doped N2200, instead of seeing new P1 and P2 peaks appear at around 0.5 and 1.5 eV upon doping, doping caused a decrease in the intensity of the BG transition with a new peak appearing at 1.4 eV and a shoulder at 1.0 eV. This opens the questions as to whether or not p- and n-doped polymers have mirror-image electronic structures and what picture, if any, can explain the spectroscopy of doped n-type polymers?

To better understand whether the traditional band picture works more universally across different types of doping and different polymers, in this paper, we extend our previous study to include both p- and n-type polymers. In particular, we perform TD-DFT calculations using hybrid functionals, both with and without long-range correction, the inclusion of counterions, and NTO analysis on both n- and p-doped P3HT and N2200. We find that for P3HT, the traditional band picture works well for understanding the electronic structure when the polymer is both p- and n-doped. However, we also see that conjugated polymers with donor−acceptor character, such as N2200, have a more complicated electronic structure that cannot be as easily reduced to a one-electronic energy level diagram. Overall, however, it still appears that if one wishes to use a one-electron picture for describing the electron structure of doped conjugated polymers, the traditional band picture still provides the best qualitatively accurate energy level diagram for explaining the observed optical transitions of most p- and n-doped semiconducting polymers.

II. COMPUTATIONAL METHODS

To determine what quantum chemistry says about the electronic structure of n- and p-doped conjugated polymers, we performed TD-DFT calculations and NTO analysis on hydrogen-terminated P3HT oligomers with 10 monomers and methyl-

https://doi.org/10.1021/acs.jctc.4c00817
J. Chem. Theory Comput. 2024, 20, 10059−10070

terminated N2200 oligomers with 3 repeat units using the Gaussian 16 package.[43] To reduce the computational cost, the P3HT hexyl side chains and N2200 alkyl chains in our calculations were replaced by methyl groups. For P3HT, we used this same oligomer length in our previous works[25,27] because we found it provided the best balance of properly describing polarons on doped P3HT (which are known experimentally to have polaron delocalization lengths of 5 to 7 monomer units)[44] while maintaining reasonable computational cost. We also performed the same calculations on P3HT oligomers with 8 and 16 monomers, with results discussed in the Supporting Information (SI). We arrive at the same one-electron energy level diagram, independent of the oligomer length. For N2200, our chosen length of 3 repeat units gives the same number of conjugated aromatic rings as P3HT with 10 monomers. All systems were geometry-optimized using DFT calculations with the 6-31G(d,p) basis set and PBE0 functional in the presence of a polarizable continuum model (PCM) with $\epsilon = 3$, chosen to match the experimentally measured dielectric constant of P3HT.[45,46]

For the geometry optimization of N2200, we fixed the dihedral angles such that the oligomer chain lies completely flat. Without fixing the dihedral angles, the optimized geometry twists around the C−C bond connecting the thiophene unit and the naphthalenetetracarboxylic diimide (NDI) unit. We performed TD-DFT calculations on both planar and nonplanar N2200 (Figure S8 in the SI), and the calculated absorption spectra are qualitatively identical. Since experiments have shown that N2200 is a preferentially face-on polymer when cast into thin films,[47] we chose to force the N2200 to be planar. The optimized P3HT and nonplanar N2200 structures have no imaginary frequencies, while the optimized planar N2200 has 14 imaginary frequencies that are less than 100 cm^{-1} due to the planar constraint. We then performed TD-DFT calculations on the optimized structures using the same basis set and functional.

Our previous work[27] showed that the use of functionals such as PBE0,[48] ωPBE[49] with default value of the range-separation parameter, and ωPBE with an optimized value of the range-separation parameter, yielded one-electron orbitals generated from NTO analysis that are qualitatively similar and which support the traditional band picture's description of the P1 and P2 transitions. We also found that the TD-DFT-calculated spectrum with the PBE0 functional gave the best agreement with experiment for p-doped P3HT. Leal et al. also found that hybrid functionals like PBE0 work better than range-separated hybrid functionals with optimized range-separation parameters for N2200 films, and that the inclusion of PCM produces a better agreement between theoretical and experimental results.[33]

Even though all this previous work suggests that the PBE0 functional should be adequate for the polymers we focus on in this work, we also performed TD-DFT calculations using the long-range-corrected ωPBE and ωB97X-D[50] functionals. For P3HT, we find that all three functionals produce the same one-electron energy level diagram, as discussed in detail in the SI. Therefore, for the rest of this paper, we will focus only on P3HT investigated with the PBE0 functional because its calculated absorption spectrum agrees best with the experimental absorption spectrum for p-doped P3HT. For N2200, as discussed in more detail below, the PBE0 and ωB97X-D functionals yield similar one-electron energy level diagrams that agree with the traditional band picture, but the ωPBE functional produces multiconfigurational transitions that cannot be easily reduced to a one-electron energy level diagram.

The main goal of this paper is to take the complex electronic structure that results from DFT (spin-split PDOS) and TD-DFT (multiconfigurational transitions that involve multiple pairs of occupied and unoccupied orbitals with different spins) calculations, and boil them down into a simplified one-electron orbital-based energy level diagram for p- and n-doped polymers that can be used as an aid to help interpret spectroscopy and other experiments. This is why we employ NTOs, which are constructed by singular value decomposition of a one-particle transition density matrix,[51,52] to simplify the assignment of TD-DFT-based optical transitions. With NTO analysis, the essential information as to what extent two electronic states involved in a transition are related to each other by a one-electron excitation is condensed into a pair of important electron/hole−particle NTOs.[53−56] Therefore, NTO analysis is specifically well-suited for orbital-based characterizations of electronic transitions and thus for constructing one-electron orbital-based energy level diagrams. NTO analysis was done using the Gaussian 16 package[43] and the orbitals were visualized using VMD[57] at isocontour values of 0.005 and −0.005.

For all the systems that we calculated, we included a point-charge counterion so that the system is electrically neutral. As mentioned above, in previous work, we showed that the position of the counterion(s) determines whether bipolarons are bound and whether two polarons will spin pair or *J*-couple.[25] We also saw that the position of the counterion(s) affects the energies of the TD-DFT calculated polaronic transitions. For this work, for our P3HT calculations, we placed a single point-charge counterion 7.5 Å from the center of the chain in the direction along the side chains. This distance was chosen to match the experimentally measured position of the anions in F_4TCNQ-doped P3HT films.[39,58,59] For N2200, we placed the counterion 7.5 Å from the center of the chain in the direction along the side chains next to the thiophene units. With this choice, the counterion sits between two bulky NDI units and thus plays a similar role to that in our P3HT calculations, allowing for ease of direct comparison. We note that there are no well-documented experimentally determined positions of the counterions in N2200 films, but we believe that the position we have chosen is the most likely location for the counterions based on steric considerations.

III. RESULTS AND DISCUSSION

We showed in previous work that the combination of TD-DFT with a hybrid functional and the inclusion of counterions gives good qualitative agreement with experiment for the ionization energies and spectral signatures of polarons, bipolarons and coupled polarons for p-doped P3HT.[25,27] The purpose of this paper is to test whether this combination also works for n-doped polymers, and to see if the underlying electronic structure better resembles the traditional band picture or the picture based on the PDOS from DFT calculations. Of course, there is no experimental spectrum of n-doped P3HT, but we can theoretically test whether p- and n-doped P3HT have identical absorption spectra with mirror-image optical transitions and electronic structures. We also theoretically examine p- and n-doped N2200, for which the experimental spectrum for the n-doped material is available (cf. Figure 2b).

III.A. Electronic Structure of p- and n-Doped p-Type P3HT. Figure 3 shows the TD-DFT-calculated absorption spectrum of both n- and p-doped P3HT using the PBE0 functional; the results and conclusions using long-range-corrected functionals are similar and are discussed in the SI. A

https://doi.org/10.1021/acs.jctc.4c00817
J. Chem. Theory Comput. 2024, 20, 10059−10070

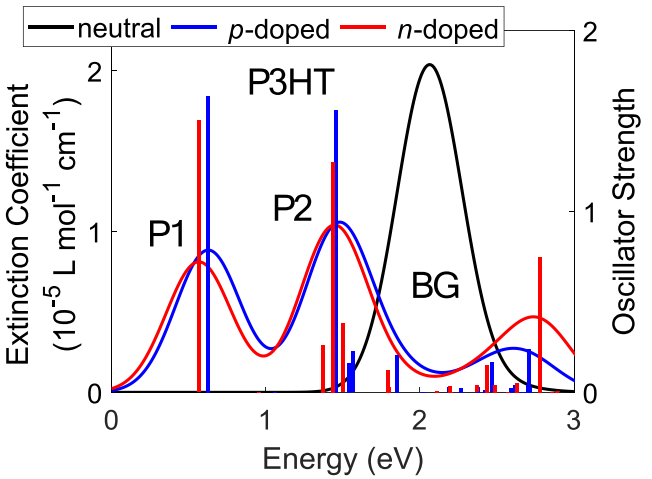

Figure 3. Absorption spectra of n- (red) and p-doped (blue) P3HT calculated with TD-DFT using the PBE0 functional and 6-31G(d,p) basis set and a counterion placed 7.5 Å from the backbone, so that the system is electrically neutral. The sticks show the individual transitions, weighted by their oscillator strength, and a width of 0.3 eV is used for plotting the absorption spectra. The calculated spectra using the ωPBE and ωB97X-D functionals are similar and are shown in Figure S3.

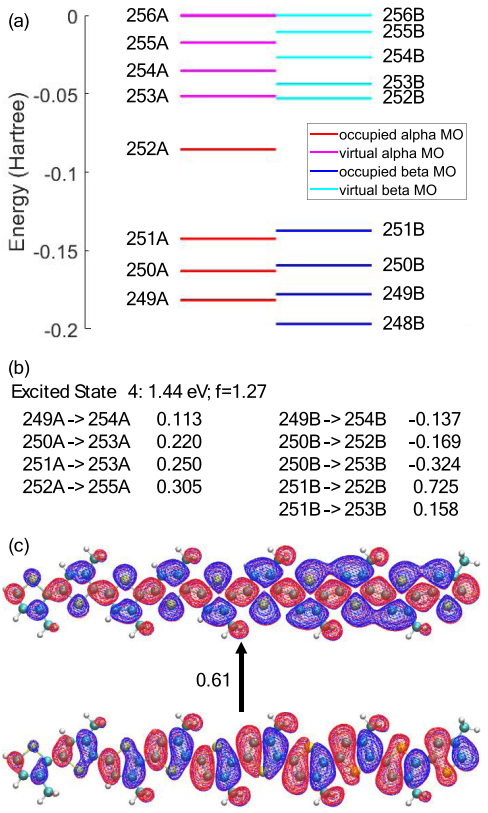

Figure 4. (a) Density of states of n-doped P3HT calculated with DFT; (b) the multiconfigurational description of the 1.44 eV electronic transition calculated with TD-DFT; (c) starting and ending one-electron natural transition orbitals for the 1.44 eV transition. In this case, the 1.44 eV electronic transition is 61% accounted for by a one-electron transition between the pictured starting and ending one-electron orbitals. All calculations were done using the PBE0 functional and 6-31G(d,p) basis set with a counterion placed 7.5 Å from the backbone so that the system is electrically neutral.

total of 20 transitions were calculated for each type of doping and a width of 0.3 eV was used for plotting the absorption spectra. The results show that both the n- and p-doped P3HT absorption spectra have nearly identical P1, P2, and BG transitions, consistent with the "mirror image" symmetry predicted by both electronic structure pictures in Figure 1. However, the underlying transitions are not entirely the same. For example, even though the n- and p-doped P2 transitions have similar energies, the P1 transition of p-doped P3HT is at a slightly higher energy than its n-doped counterpart, and for both the P1 and P2 transitions, the oscillator strength is slightly higher for p-doped P3HT than for n-doped P3HT. In addition to the P1 and P2 transitions, TD-DFT calculations yield several other transitions with low oscillator strengths, but these transitions would not be visible experimentally under the strongly allowed P2 transition, so as discussed further in the SI, we do not include them below when constructing our simplified one-electron energy level diagrams.[27]

Figure 4a shows the DFT projected density of states for n-doped P3HT; as has been seen in previous work and summarized in Figure 1b, the PDOS appears to show a single spin-split occupied state (252A) that stands out from the others. It is unclear, however, whether one should assign this state as the only state lying in the gap or if there are other states in the gap. As we show in the SI for p- and n-doped P3HT, however, if one uses the TD-DFT-calculated energy diagram or DFT-calculations on a pair of π-stacked P3HT chains to identify how doping shifts the edges of the valence and conduction bands, the PDOS also appears to be "traditional band picture"-like in that there are two states that lie in the gap. Both the TD-DFT-calculated energy diagram from our previous work[27] and this work, and the DFT calculations on a pair of doped π-stacked P3HT chains in the SI, show that p-doping shifts only the edge of valence band, while n-doping shifts only the edge of the conduction band. This has important consequences for interpreting the PDOS. For example, because n-doping shifts only the position of the conduction band and not the valence band, the result is that both states 251A and 251B are also in the gap. By placing states 251 and 252 in the gap, the resulting energy level diagram agrees with the traditional band picture. We also note that TD-DFT calculations, which provide a much better description of the electronic excited states that are involved in optical transitions, also have an electronic structure that matches energy level diagram from the traditional band picture.

Figure 4b shows the TD-DFT-calculated electronic structure for the transition at 1.44 eV for n-doped P3HT. The multiconfigurational description makes any simple assignment of this transition challenging, as there is no single pair of energy levels in the PDOS that can explain the origin of this transition. Thus, we turn to NTO analysis to simplify the assignment of the TD-DFT-based optical transitions, because the construction of NTOs condenses the essential information on an optical transition into a quasi-one-electron excitation between a pair of important electron/hole-particle orbitals, which for the 1.44 eV transition are shown in Figure 4c.

Figure 5 shows the one-electron NTOs associated with the P1, P2, P3, P3′, and BG transitions for p- and n-doped P3HT. For most of the transitions, the natural transition orbital coefficients are greater than 50%, which means that these transitions can be fairly well approximated by the transition of a single electron between the starting and the ending orbitals. We see that the oscillator strengths of the symmetry-forbidden P3

https://doi.org/10.1021/acs.jctc.4c00817
J. Chem. Theory Comput. 2024, 20, 10059−10070

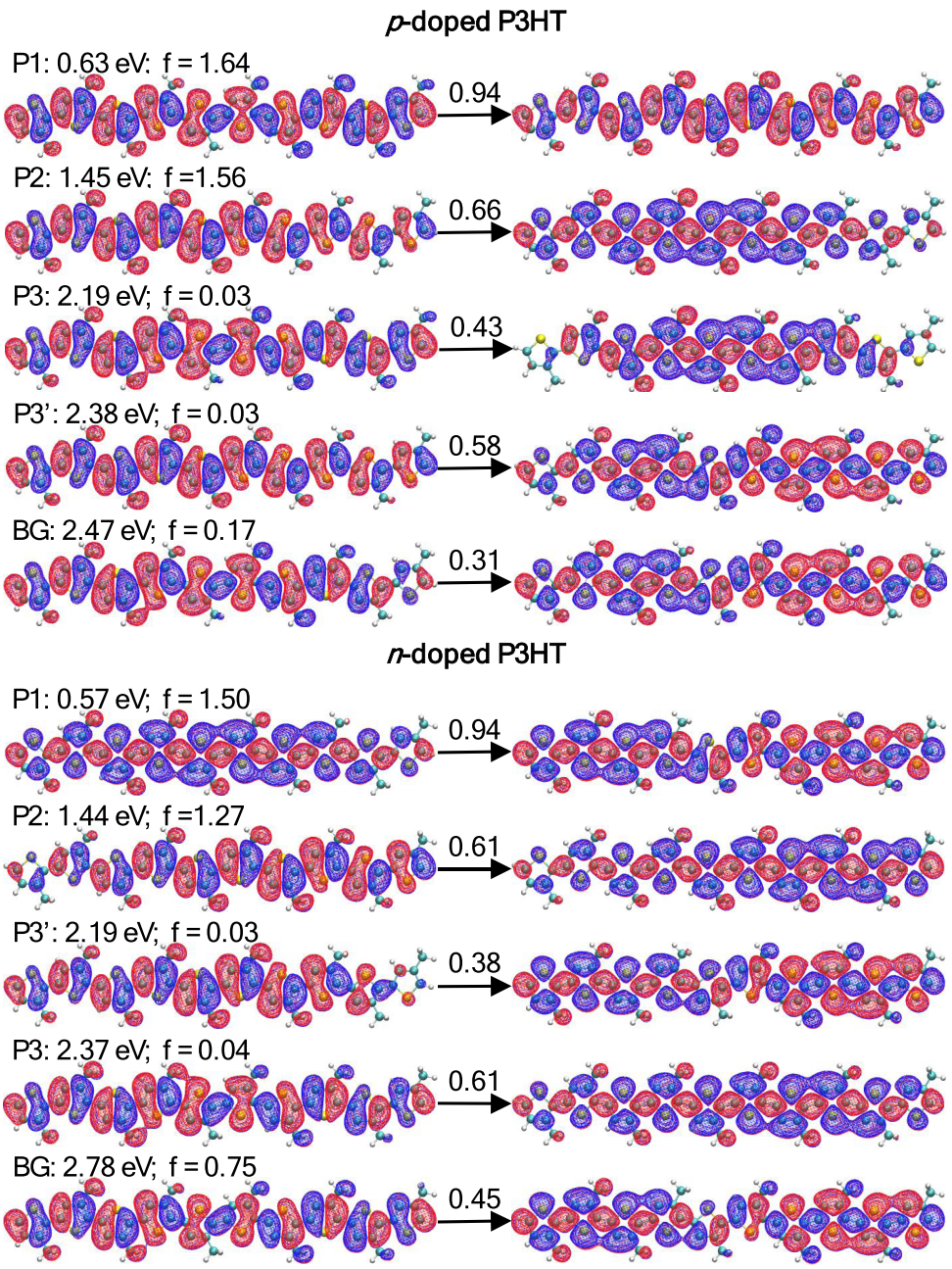

Figure 5. Starting and ending one-electron orbitals for the P1, P2, P3, P3′, and BG transitions generated from NTO analysis of our PBE0/6-31G(p,d) TD-DFT calculations on p- and n-doped P3HT. As in Figure 4, the numbers above the arrows are the NTO coefficients between the orbital pairs connected by the arrows. The identity, energy, and oscillator strength are shown above and to the left of each transition.

and P3′ transitions are much smaller than the P1, P2, and BG transitions, as expected with the traditional band picture.

One of the key ideas of this work is to use NTOs to construct a one-electron energy level diagram, which requires determining when the NTOs associated with different transitions are essentially the same. Thus, to compare NTOs, we calculated their orbital overlaps. For example, to compare the ending orbital of the P1 transition and the starting orbital of the P2 transition, the orbital overlap is calculated by

$$\text{overlap} = \left| \int \Psi_{\text{P1,end}} \Psi_{\text{P2,start}} d\mathbf{r} \right| \quad (2)$$

where the absolute value accounts for the fact that the calculated phase of the orbitals is arbitrary, which could give a negative result when the phase is flipped. A detailed explanation of our calculation of the NTO overlaps is included in the SI. Since the orbitals are normalized, an overlap of 1 means that the two orbitals are identical, whereas an overlap of 0 means that the two orbitals are completely orthogonal. Tables S2 and S3 in the SI list the overlaps of all the orbitals involved in the P1, P2, P3, P3′, and BG transitions for p- and n-doped P3HT, respectively.

As we discussed in our previous work, the NTOs for p-doped P3HT (upper part of Figure 5) have essentially identical starting orbitals for the BG and P1 transitions, with an overlap of 0.93. They also show that the ending orbital of the P1 transition is very similar to the starting orbital of the P2 transition, with an overlap of 0.92.[27] We also see that the NTOs associated with the low-oscillator-strength P3 and P3′ transitions use essentially these

https://doi.org/10.1021/acs.jctc.4c00817
J. Chem. Theory Comput. 2024, 20, 10059−10070

same orbitals (overlaps ≥0.92), all in a way that is consistent with the traditional band picture.[27]

The lower portion of Figure 5 shows that for n-doped P3HT, the ending orbital of the P2 transition matches the starting orbital of the P1 transition, with an overlap of 0.87. We also see that the starting orbital of the P3′ transition matches the starting orbital of the P2 transition, with an overlap of 0.97, and that the ending orbital of the P3′ transition matches the ending orbital of the P1 transition, with an overlap of 0.95. The NTOs associated with the BG transition also match the starting orbital of the P3 transition, with an overlap of 0.96, and the ending orbital of the P1 transition, with an overlap of 0.97. All of these features are consistent with the traditional band picture in Figure 1a, and are in disagreement with the DFT PDOS-based model in Figure 1b.

Perhaps most importantly, Figure 5 shows that p- and n-doped P3HT have essentially the same starting and ending orbitals for both the BG and P2 transitions. The overlaps of the starting and ending orbitals of the p-doped P2 transition with that of the n-doped P2 transition are 0.71 and 0.66, respectively. The overlaps of the starting and ending orbitals of the p-type BG transition with that of the n-doped BG transition are 0.83 and 0.72, respectively. The orbital overlaps of the NTOs for p-doped P3HT with the NTOs for n-doped P3HT are listed in Table S4. This allows us to identify common energy levels between the two types of doping, something that is not possible with the PDOS from separate DFT calculations.

By aligning the common orbitals as belonging to the same one-electron energy levels and then spacing the levels according to the associated TD-DFT transition energies, we can build a one-electron energy level diagram, which is shown in Figure 6.

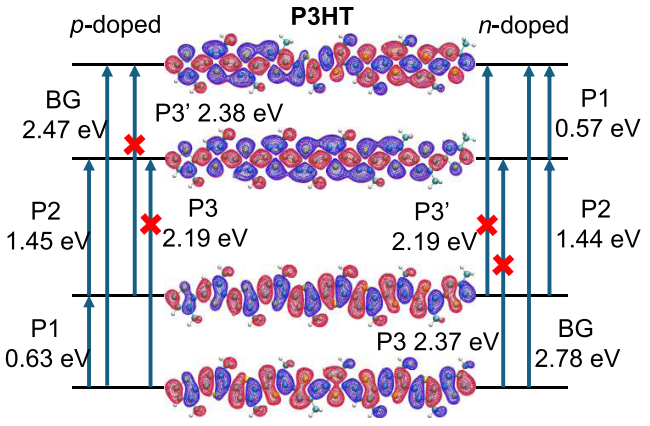

Figure 6. Effective one-electron energy level diagram and one-electron transitions based on TD-DFT and NTO matching for n- and p-doped P3HT, which agrees with the traditional band picture.

The energy level diagram matches well with the traditional band picture, although we do see some minor differences. For example, the energies of the transitions are slightly different for the n- and p-doped polymer, although these differences are small and likely reflect the fact that the transitions are multiconfigurational in character and thus not perfectly represented by a one-electron picture. Overall, we conclude that if one wishes to draw a one-electron picture to describe n- and p-doped P3HT, the traditional band picture provides a much better way to understand the spectroscopy and electronic structure than the DFT-based PDOS model.

III.B. Electronic Structure of p- and n-Doped n-Type N2200. Having established that the use of TD-DFT calculations with NTO analysis for both n- and p-doped P3HT yields an electronic structure that agrees well with the one-electron traditional band picture, we now turn our attention to a commonly studied n-type polymer, N2200. The TD-DFT-calculated absorption spectra of p- and n-doped N2200 are shown in Figure 7a. Unlike what we saw for P3HT, the

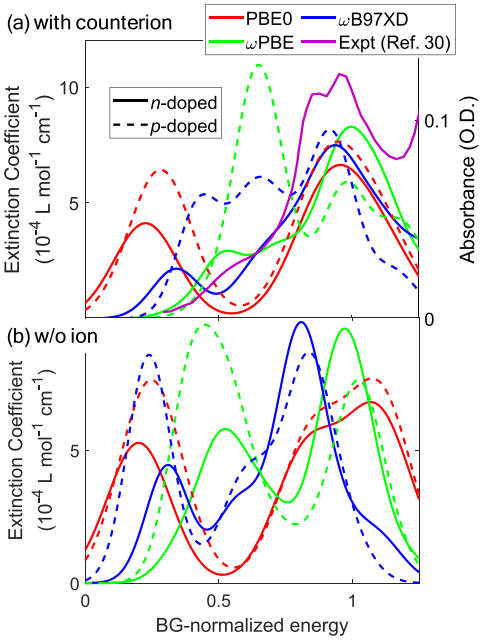

Figure 7. Absorption spectra of p- (dashed curves) and n-doped (solid curves) N2200 (a) with and (b) without a counterion, calculated with TD-DFT using the PBE0 (red curves), ωPBE (green curves), and ωB97X-D (blue curves) functionals and 6-31G(d,p) basis set. For the calculations in (a), the counterion is placed 7.5 Å from the center of the chain in the direction along the side chains next to the thiophene units. A width of 0.3 eV is used for plotting the absorption spectra. The *x*-axis is scaled by the energy of the BG transition of the neutral (undoped) N2200; nonscaled spectra are included in the SI. The experimental absorption spectrum is reproduced from ref 31 and is the same as the one shown in Figure 2b but scaled to the energy of the BG transition. The experimental N2200 film was doped with N-DMBI, a commonly used dopant for n-type polymers.

calculated spectra for n-doped N2200 are different for the three different functionals we employed. Since the three functionals yielded three different bandgap transitions for this material, we plot the spectra on an energy scale (x) normalized to the BG transition energy for ease of comparison; the unscaled spectra are included in the SI. Moreover, also unlike P3HT, the lowest energy P1-like transitions of n- and p-doped N2200 do not occur at the same relative energy and have different oscillator strengths. This difference between the n- and p-doped calculated spectra is particularly exaggerated when using the ωPBE and ωB97X-D functionals, suggesting that p- and n-doped N2200 do not have mirror-image electronic structures.

The calculated spectra of n-doped N2200 in Figure 7a also do not have clearly distinct P1, P2, and BG peaks. Instead, they show only two main peaks: one near the neutral BG transition and one below the neutral BG transition. The PBE0 functional predicts that the peak below the neutral BG transition is the most red-shifted, whereas ωPBE gives the most blue-shifted peak. The calculated spectra using the ωPBE and ωB97X-D functionals also have a shoulder near x = 0.7. Of the three

https://doi.org/10.1021/acs.jctc.4c00817
J. Chem. Theory Comput. 2024, 20, 10059−10070

functionals we used, the spectra calculated using the ωPBE and ωB97X-D functionals look the most similar to the experimental absorption spectrum of n-doped N2200 reported in ref 31 and shown in Figure 2b; this experimental spectrum is also reproduced scaled to the bandgap energy in Figure 7a (purple curve). For undoped N2200, the calculated spectrum using the PBE0 functional agrees the best with the experimental spectrum (see the SI). All of these observations suggest that there are important differences between the electronic structures of doped N2200 and doped P3HT.

First, we explore the reasons why p- and n-doped N2200 do not have mirror-image electronic structures. Unlike P3HT, N2200 is a donor−acceptor-type polymer composed of thiophene units, which are electron rich, and NDI units, which are electron poor. Therefore, when N2200 is oxidized or reduced, the hole and the electron prefer to reside on different subunits. This is quantified in Figure 8, which shows the

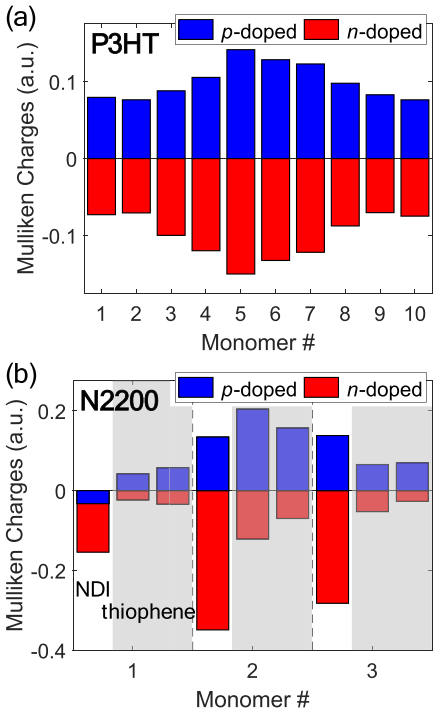

Figure 8. Distribution of DFT-calculated Mulliken charges for n- and p-doped (a) P3HT and (b) N2200 using the PBE0 functional. For N2200, the shaded regions denote the thiophene units and the unshaded regions the NDI units. For P3HT, the charge distributions are essentially identical for n- and p-doping, but for N2200, a donor−acceptor-type polymer, the charge distributions are different for n- and p-doping. Mulliken charge distributions for other functionals are shown in the SI.

distribution of Mulliken charges for n- and p-doped P3HT (panel a) and N2200 (panel b) using the PBE0 functional. The distribution of Mulliken charges for n- and p-doped N2200 using the ωPBE and ωB97X-D functionals are similar to that using the PBE0 functional, as shown in Figure S4 in the SI. The charge distributions are essentially identical for n- and p-doped P3HT, but clearly quite different for n- and p-doped N2200. As expected, the positive hole resides mainly on the electron-rich thiophene units in p-doped N2200, while the negative electron strongly prefers to reside on the electron-poor NDI units in the n-doped material. Not only do the polarons of different signs reside on different subunits, but they also have different degrees of delocalization, explaining why the P1-like transitions have different energies.

Moreover, the fact that N2200 is a donor−acceptor-type polymer also explains why different functionals produced different calculated spectra for doped N2200 but not for doped P3HT. Many studies have shown that TD-DFT often fails to correctly describe charge-transfer excitations.[60−64] Since N2200 is a donor−acceptor-type polymer, its excitations have charge-transfer character, explaining why different functionals give different results. Since P3HT is not a donor−acceptor-type polymer, its excitations have little charge-transfer character, consistent with the fact that all three functionals yield essentially the same result.

The other significant difference between P3HT and N2200 comes in the relative positions of the dopant counterions. For n-doped N2200, the positive counterion sits between two NDI subunits, forcing the electron to at least partially sit on the more electron-rich thiophene subunits. Figure 7b shows that when the counterions are removed, the calculated spectra of p- and n-doped N2200 become more similar. However, the spectra are still not as similar as those for p- and n-doped P3HT (Figure 3) because even without the counterions, the presence of separate electron-rich and electron-poor subunits makes the electronic structures of p- and n-doped N2200 different.

To determine if the assignments of the optical transitions by the traditional band picture model also work qualitatively for n-doped N2200, we constructed a one-electron description of the energy level diagram using NTOs along the same lines as we did in the previous section for P3HT.[27] To minimize the complications that arise from the presence and the location of the counterion, we performed our NTO analysis on the TD-DFT calculations without counterion. If n-doped N2200 behaves in the same way as n-doped P3HT, then the ending orbital of the P2-like transition should be essentially the same as the starting orbital of the P1-like transition. Therefore, to identify whether an N2200 transition is P2-like, we calculated the orbital overlaps of the starting orbital of the P1-like transition (denoted by * in Figure 9a) with the ending orbital of the different calculated transitions.

For the PBE0 functional, there are multiple N2200 transitions (denoted by ** in Figure 9a) whose ending orbitals are the same as the starting orbitals of the P1-like transition, with overlaps of 0.90, 0.94, and 0.67. For the P2-like transition with an ending orbital overlap of 0.67, the ending orbital is localized on the middle NDI and thiophene units rather than delocalized across multiple NDI units as with the other two P2-like transitions. For the ωB97X-D functional, the ending orbital of the strongly allowed transition near x = 0.8 (denoted by ** in Figure 9b) is the same as the starting orbital of the P1-like transition with an overlap of 0.84. Figure 9b shows the effective starting and ending one-electron orbitals and the NTO coefficients of the P1-like and P2-like transitions for these two functionals.

Thus, the broad peak at x = 0.8 in the TD-DFT-calculated spectra using both the PBE0 and ωB97X-D functionals is indeed P2-like in the language of the traditional band picture, even though in the experimental spectrum, it appears more as a shoulder on the BG transition. The natural transition orbital coefficients (Figure 9b) for the P2-like transitions using both PBE0 and ωB97X-D functionals are around 0.3. These coefficients indicate that these transitions are much less "one-electron-like" than the P2 transitions in doped P3HT, suggesting that things are more complicated for donor−acceptor-type conjugated polymers because of issues with asymmetry.

https://doi.org/10.1021/acs.jctc.4c00817
J. Chem. Theory Comput. 2024, 20, 10059−10070

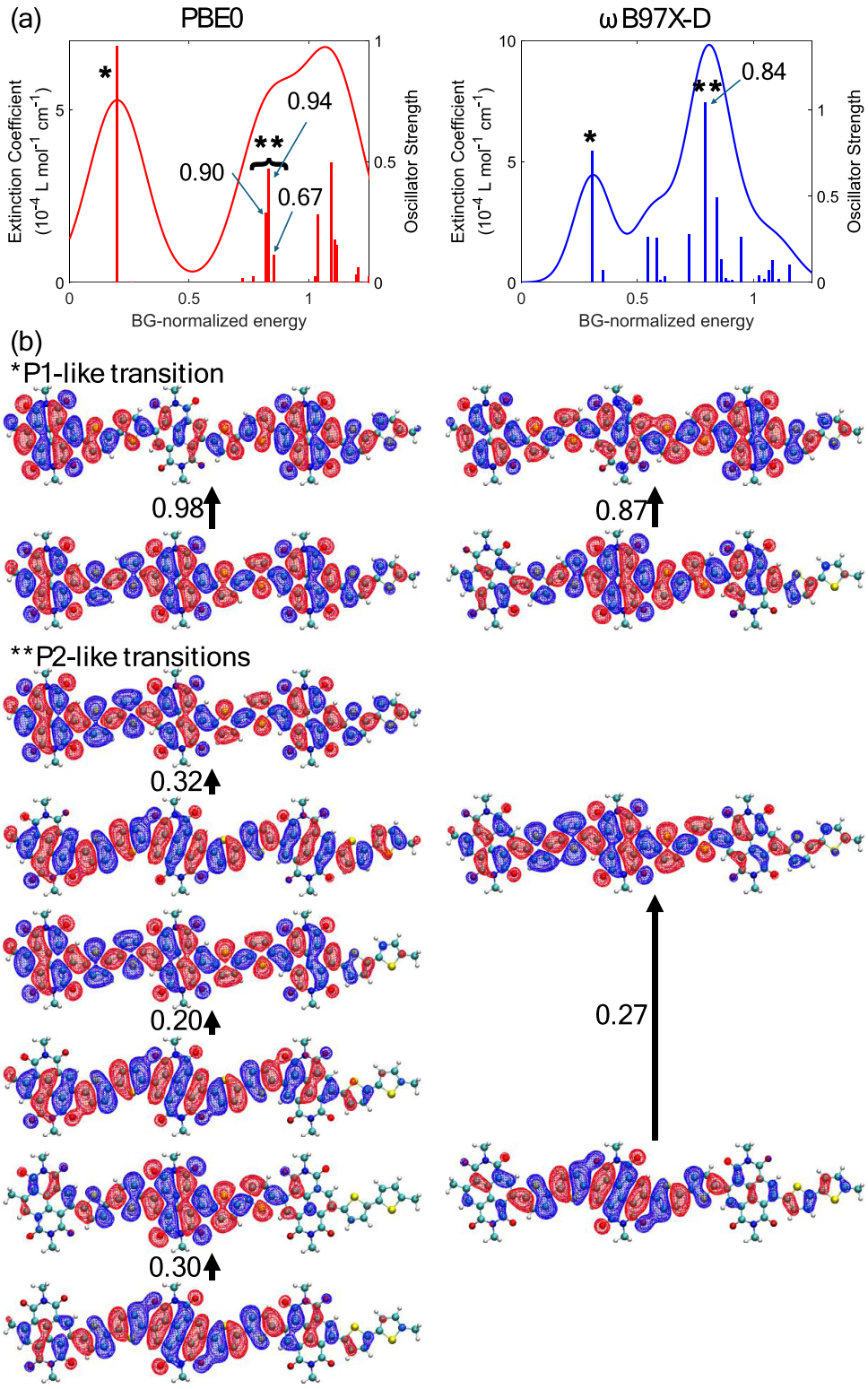

Figure 9. (a) Absorption spectra of n-doped N2200 calculated using the PBE0 functional (left) and the ωB97X-D functional (right). The P1-like and P2-like transitions are marked with * and **, respectively. For the P2-like transitions, the orbital overlaps of their ending orbitals with the starting orbital of the P1 transition are listed in the absorption spectra with arrows pointing to the transitions. The sticks show the individual transitions, weighted by their oscillator strength, and a width of 0.3 eV is used for plotting the absorption spectra. (b) Starting and ending one-electron orbitals from NTO analysis of the P1-like and P2-like transitions of n-doped N2200 calculated using the PBE0 functional (left column) and the ωB97X-D functional (right column). The numbers next to the black arrows connecting the orbitals are the NTO coefficients between the orbital pairs connected by the arrows.

However, the basic features of the traditional picture still appear to work fairly well in describing the electronic structure.

For the ωPBE functional, we find that the multiconfigurational TD-DFT electronic transitions cannot be easily reduced

https://doi.org/10.1021/acs.jctc.4c00817
J. Chem. Theory Comput. 2024, 20, 10059−10070

to a one-electron energy level diagram for two reasons. First, the transitions are simply not "one-electron-like". Of the 20 electronic transitions calculated, only four transitions have NTO coefficients greater than 0.4, and none of the transitions have an NTO coefficient greater than 0.6. Second, the orbital overlaps indicate that most of the transitions with significant oscillator strength have essentially the same starting orbital, which would give a one-electron energy level diagram that is different from both the traditional band picture and the DFT-based PDOS model, as discussed in the SI.

Finally, we address the question of why the experimental spectrum of doped N2200 in Figure 7a (the same as non-BG-normalized spectrum shown in Figure 2b) does not show a P1-like transition? For the calculated spectra, the P1-like transition for n-doped N2200 is at x = 0.22 and 0.34 for the PBE0 and ωB97X-D functionals, respectively, but the experimental spectrum of doped N2200 appears to not have any absorption below x = 0.4. We see three possible explanations. First, as mentioned above, TD-DFT-calculated transitions tend to be blue-shifted compared to experiment.[65−67] This means that there could be a P1-like transition in the experiment that is beyond the red edge of the figure and thus was not visible to Guo et al.[31] Second, it is now well documented that strong Coulomb interactions between the counterion and polaron can blue-shift the polaron's P1 absorption.[25,26,39] Thus, it is possible that the shoulder at x = 0.5 in the experimental spectrum in Figure 7a (purple curve) could be the P1-like transition we see in our calculations but blue-shifted by a counterion interaction that is stronger than what we included in our calculations. Finally, in the experiment, N2200 was doped using *N*-DMBI (4-(2,3-dihydro-1,3-dimethyl-1*H*-benzimidazol-2-yl)-*N*,*N*-dimethylbenzenamine; see Figure 2c for chemical structure), which instead of transferring an electron to the polymer as in our calculations, dopes the polymer via hydride transfer.[68] In addition to doping, the hydride transfer reaction might break the conjugation of the polymer backbone or otherwise alter the chemical and electronic structure in ways that are not accounted for in our calculations. Regardless, the experimental spectra of the other n-doped polymers in Figure 2b, PDTzTI and BTI2TEG-FT, do show P1 and P2 peaks that strongly resemble the experimental spectrum of p-doped P3HT and the calculated spectrum of n-doped P3HT. This suggests that the absence of a P1-like transition in N2200 is likely an exception and worth further exploration.

We close by noting that our NTO and energy level analysis can directly be tested by pump−probe spectroscopy. The energy-level diagram from the PBE0 and ωB97X-D functionals predicts that if one were to pump the P2-like transition of n-doped N2200, it would cause an induced absorption of the P1-like transition, whereas if one pumps the BG transition, it would not cause any induced absorption. One could then tune the pump wavelength to create an action spectrum to map out the underlying P2-like and BG transitions in much the same way as we did previously to map out the different P1 spectra of free and trapped polarons in doped P3HT.[14] The model based on the DFT PDOS, in contrast, predicts that exciting either the P2-like or BG transitions of n-doped N2200 should have no effect on any of the other transitions. Thus, our conclusion is that even though the transitions in doped N2200 are less "one-electron-like" and much more subject to counterion effects, the traditional band picture still serves as the most useful simple energy level diagram for understanding electronic structure, an idea that can be directly tested by experiment.

IV. CONCLUSIONS

In this paper, we used TD-DFT calculations to better understand the electronic structure of p- and n-doped conjugated polymers. We find that by using NTOs to construct the best possible one-electron energy level diagram, we end up obtaining the traditional band picture. Of course, our calculations do not include the reorganization that accompanies the excitation of one of the doped polymer transitions (the so-called Hubbard U),[13] and they can only approximately account for the multiconfigurational character involved in systems with many correlated electrons in the conjugated π system. But to the extent that it is useful to have a simple one-electron picture for the electronic structure of doped polymers, our calculations indicate that the traditional picture is superior to the one based on the DFT-calculated projected density of states.

We also saw that the situation is more complicated for donor−acceptor-type polymers, particularly when the dopant counterions are explicitly accounted for. This is because the symmetry between n- and p-doping is broken by the facts that the different polarons prefer to reside on different subunits and that there is typically only one place for the counterion to sit in the polymer lattice; this causes the two types of doping to no longer be mirror images. Our calculations based on hybrid and long-range-corrected hybrid functionals provide a definitive prediction for the results of pump−probe experiments on n-doped conjugated polymers that could be used to test the origins of the underlying optical transitions. Overall, we believe that the traditional band picture still provides a qualitatively accurate understanding of the electronic structure of doped conjugated polymers no matter whether they are p- or n-doped and whether the polymer has push−pull character or not.

■ ASSOCIATED CONTENT

Supporting Information

The Supporting Information is available free of charge at https://pubs.acs.org/doi/10.1021/acs.jctc.4c00817.

Additional calculation details, convergence study on the sensitivity of the results to oligomer length, and results with long-range-corrected functionals (PDF)

■ AUTHOR INFORMATION

Corresponding Authors

Eric C. Wu − *Department of Chemistry and Biochemistry, University of California, Los Angeles, Los Angeles, California 90095-1569, United States*; Email: wuericck@gmail.com

Benjamin J. Schwartz − *Department of Chemistry and Biochemistry, University of California, Los Angeles, Los Angeles, California 90095-1569, United States*; orcid.org/0000-0003-3257-9152; Email: schwartz@chem.ucla.edu

Complete contact information is available at: https://pubs.acs.org/10.1021/acs.jctc.4c00817

Notes

The authors declare no competing financial interest.

■ ACKNOWLEDGMENTS

This work was supported by the National Science Foundation under grants CHE-2305152 and DMR-2105896.

REFERENCES

(1) Bredas, J. L.; Street, G. B. Polarons, Bipolarons, and Solitons in Conducting Polymers. *Acc. Chem. Res.* **1985**, *18* (10), 309−315.
(2) Nowak, M.; Rughooputh, S. D. D. V.; Hotta, S.; Heeger, A. J. Polarons and Bipolarons on a Conducting Polymer in Solution. *Macromolecules* **1987**, *20* (5), 965−968.
(3) Beljonne, D.; Cornil, J.; Sirringhaus, H.; Brown, P. J.; Shkunov, M.; Friend, R. H.; Brédas, J.-L. Optical Signature of Delocalized Polarons in Conjugated Polymers. *Adv. Funct. Mater.* **2001**, *11* (3), 229−234.
(4) Bubnova, O.; Khan, Z. U.; Wang, H.; Braun, S.; Evans, D. R.; Fabretto, M.; Hojati-Talemi, P.; Dagnelund, D.; Arlin, J.-B.; Geerts, Y. H.; Desbief, S.; Breiby, D. W.; Andreasen, J. W.; Lazzaroni, R.; Chen, W. M.; Zozoulenko, I.; Fahlman, M.; Murphy, P. J.; Berggren, M.; Crispin, X. Semi-Metallic Polymers. *Nat. Mater.* **2014**, *13* (2), 190−194.
(5) Fichou, D.; Horowitz, G.; Xu, B.; Garnier, F. Stoichiometric Control of the Successive Generation of the Radical Cation and Dication of Extended α-Conjugated Oligothiophenes: A Quantitative Model for Doped Polythiophene. *Synth. Met.* **1990**, *39* (2), 243−259.
(6) Kahmann, S.; Loi, M. A.; Brabec, C. J. Delocalisation Softens Polaron Electronic Transitions and Vibrational Modes in Conjugated Polymers. *J. Mater. Chem. C* **2018**, *6* (22), 6008−6013.
(7) Campbell, D. K.; Bishop, A. R.; Fesser, K. Polarons in Quasi-One-Dimensional Systems. *Phys. Rev. B* **1982**, *26* (12), No. 6862.
(8) Chung, T.-C.; Kaufman, J. H.; Heeger, A. J.; Wudl, F. Charge Storage in Doped Poly(Thiophene): Optical and Electrochemical Studies. *Phys. Rev. B* **1984**, *30* (2), No. 702.
(9) Kaloni, T. P.; Giesbrecht, P. K.; Schreckenbach, G.; Freund, M. S. Polythiophene: From Fundamental Perspectives to Applications. *Chem. Mater.* **2017**, *29* (24), 10248−10283.
(10) Heimel, G. The Optical Signature of Charges in Conjugated Polymers. *ACS Cent. Sci.* **2016**, *2* (5), 309−315.
(11) Zozoulenko, I.; Singh, A.; Singh, S. K.; Gueskine, V.; Crispin, X.; Berggren, M. Polarons, Bipolarons, And Absorption Spectroscopy of PEDOT. *ACS Appl. Polym. Mater.* **2019**, *1* (1), 83−94.
(12) Sahalianov, I.; Hynynen, J.; Barlow, S.; Marder, S. R.; Müller, C.; Zozoulenko, I. UV-to-IR Absorption of Molecularly p-Doped Polythiophenes with Alkyl and Oligoether Side Chains: Experiment and Interpretation Based on Density Functional Theory. *J. Phys. Chem. B* **2020**, *124* (49), 11280−11293.
(13) Lungwitz, D.; Joy, S.; Mansour, A. E.; Opitz, A.; Karunasena, C.; Li, H.; Panjwani, N. A.; Moudgil, K.; Tang, K.; Behrends, J.; Barlow, S.; Marder, S. R.; Brédas, J.-L.; Graham, K.; Koch, N.; Kahn, A. Spectral Signatures of a Negative Polaron in a Doped Polymer Semiconductor: Energy Levels and Hubbard *U* Interactions. *J. Phys. Chem. Lett.* **2023**, *14* (24), 5633−5640.
(14) Voss, M. G.; Scholes, D. T.; Challa, J. R.; Schwartz, B. J. Ultrafast Transient Absorption Spectroscopy of Doped P3HT Films: Distinguishing Free and Trapped Polarons. *Faraday Discuss.* **2019**, *216*, 339−362.
(15) Umar, A. R.; Dorris, A. L.; Kotadiya, N. M.; Giebink, N. C.; Collier, G. S.; Grieco, C. Probing Polaron Environment in a Doped Polymer via the Photoinduced Stark Effect. *J. Phys. Chem. C* **2023**, *127* (20), 9498−9508.
(16) Voss, M. G.; Challa, J. R.; Scholes, D. T.; Yee, P. Y.; Wu, E. C.; Liu, X.; Park, S. J.; León Ruiz, O.; Subramaniyan, S.; Chen, M.; Jenekhe, S. A.; Wang, X.; Tolbert, S. H.; Schwartz, B. J. Driving Force and Optical Signatures of Bipolaron Formation in Chemically Doped Conjugated Polymers. *Adv. Mater.* **2021**, *33* (3), No. 2000228.
(17) Umar, A. R.; Dorris, A. L.; Grieco, C. Photoexcited Polaron Relaxation as a Structurally Sensitive Reporter of Charge Trapping in a Conducting Polymer. *Adv. Funct. Mater.* **2024**, No. 2407181.
(18) Wen, G.; Zou, X.; Hu, R.; Peng, J.; Chen, Z.; He, X.; Dong, G.; Zhang, W. Ground- and Excited-State Characteristics in Photovoltaic Polymer N2200. *RSC Adv.* **2021**, *11* (33), 20191−20199.
(19) Gish, M. K.; Karunasena, C. D.; Carr, J. M.; Kopcha, W. P.; Greenaway, A. L.; Mohapatra, A. A.; Zhang, J.; Basu, A.; Brosius, V.; Pratik, S. M.; Bredas, J.-L.; Coropceanu, V.; Barlow, S.; Marder, S. R.; Ferguson, A. J.; Reid, O. G. The Excited-State Lifetime of Poly(NDI2OD-T2) Is Intrinsically Short. *J. Phys. Chem. C* **2024**, *128* (15), 6392−6400.
(20) Cornil, J.; Brédas, J. Nature of the Optical Transitions in Charged Oligothiophenes. *Adv. Mater.* **1995**, *7* (3), 295−297.
(21) Aubry, T. J.; Winchell, K. J.; Salamat, C. Z.; Basile, V. M.; Lindemuth, J. R.; Stauber, J. M.; Axtell, J. C.; Kubena, R. M.; Phan, M. D.; Bird, M. J.; Spokoyny, A. M.; Tolbert, S. H.; Schwartz, B. J. Tunable Dopants with Intrinsic Counterion Separation Reveal the Effects of Electron Affinity on Dopant Intercalation and Free Carrier Production in Sequentially Doped Conjugated Polymer Films. *Adv. Funct. Mater.* **2020**, *30* (28), No. 2001800.
(22) Wang, C.; Duong, D. T.; Vandewal, K.; Rivnay, J.; Salleo, A. Optical Measurement of Doping Efficiency in Poly(3-Hexylthiophene) Solutions and Thin Films. *Phys. Rev. B* **2015**, *91* (8), No. 085205.
(23) Nagamatsu, S.; Pandey, S. S. Ordered Arrangement of F4TCNQ Anions in Three-Dimensionally Oriented P3HT Thin Films. *Sci. Rep.* **2020**, *10* (1), No. 20020.
(24) Brown, P. J.; Sirringhaus, H.; Harrison, M.; Shkunov, M.; Friend, R. H. Optical Spectroscopy of Field-Induced Charge in Self-Organized High Mobility Poly(3-Hexylthiophene). *Phys. Rev. B* **2001**, *63* (12), No. 125204.
(25) Wu, E. C.; Salamat, C. Z.; Ruiz, O. L.; Qu, T.; Kim, A.; Tolbert, S. H.; Schwartz, B. J. Counterion Control and the Spectral Signatures of Polarons, Coupled Polarons, and Bipolarons in Doped P3HT Films. *Adv. Funct. Mater.* **2023**, *33*, No. 2213652.
(26) Aubry, T. J.; Axtell, J. C.; Basile, V. M.; Winchell, K. J.; Lindemuth, J. R.; Porter, T. M.; Liu, J.; Alexandrova, A. N.; Kubiak, C. P.; Tolbert, S. H.; Spokoyny, A. M.; Schwartz, B. J. Dodecaborane-Based Dopants Designed to Shield Anion Electrostatics Lead to Increased Carrier Mobility in a Doped Conjugated Polymer. *Adv. Mater.* **2019**, *31* (11), No. 1805647.
(27) Wu, E. C.; Schwartz, B. J. Does the Traditional Band Picture Describe the Electronic Structure of Doped Conjugated Polymers? TD-DFT and Natural Transition Orbital Study of Doped P3HT. *J. Chem. Theory Comput.* **2023**, *19* (19), 6761−6769.
(28) Yang, C.-Y.; Ding, Y.-F.; Huang, D.; Wang, J.; Yao, Z.-F.; Huang, C.-X.; Lu, Y.; Un, H.-I.; Zhuang, F.-D.; Dou, J.-H.; Di, C.; Zhu, D.; Wang, J.-Y.; Lei, T.; Pei, J. A Thermally Activated and Highly Miscible Dopant for N-Type Organic Thermoelectrics. *Nat. Commun.* **2020**, *11* (1), No. 3292.
(29) Matsuo, T.; Kawabata, K.; Takimiya, K. Highly Electron-Donating Bipyranylidene Derivatives: Potential n-Type Dopants for Organic Thermoelectrics. *Adv. Energy Sustainability Res.* **2021**, *2* (11), No. 2100084.
(30) Liu, J.; Qiu, L.; Alessandri, R.; Qiu, X.; Portale, G.; Dong, J.; Talsma, W.; Ye, G.; Sengrian, A. A.; Souza, P. C. T.; Loi, M. A.; Chiechi, R. C.; Marrink, S. J.; Hummelen, J. C.; Koster, L. J. A. Enhancing Molecular n-Type Doping of Donor−Acceptor Copolymers by Tailoring Side Chains. *Adv. Mater.* **2018**, *30* (7), No. 1704630.
(31) Guo, H.; Yang, C.-Y.; Zhang, X.; Motta, A.; Feng, K.; Xia, Y.; Shi, Y.; Wu, Z.; Yang, K.; Chen, J.; Liao, Q.; Tang, Y.; Sun, H.; Woo, H. Y.; Fabiano, S.; Facchetti, A.; Guo, X. Transition Metal-Catalysed Molecular n-Doping of Organic Semiconductors. *Nature* **2021**, *599* (7883), 67−73.
(32) Magnanelli, T. J.; Heilweil, E. J. Charge Conductivity in Donor−Acceptor Polymer Dispersions Measured with Time-Resolved Terahertz Spectroscopy. *Chem. Phys.* **2021**, *540*, No. 111005.
(33) Leal, L. A.; de Sousa, L. E.; de Brito, P. P.; Neto, B. G. E.; Ceschin, A. M.; da Cunha, W. F.; Ribeiro, L. A.; da Silva Filho, D. A. Optical Properties of P3HT and N2200 Polymers: A Performance Study of an Optimally Tuned DFT Functional. *J. Mol. Model.* **2018**, *24* (1), No. 32.
(34) Ledo, R. M. D.; Leal, L. A.; De Brito Silva, P. P.; Da Cunha, W. F.; De Souza, L. E.; Fonseca, A. L. A.; Ceschin, A. M.; Da Silva Filho, D. A.; Ribeiro, L. A., Junior Modeling Optical Properties of Polymer−Solvent Complexes: The Chloroform Influence on the P3HT and N2200 Absorption Spectra. *J. Mol. Model.* **2017**, *23* (2), No. 37.
(35) Pankow, R. M.; Wu, J.; Harbuzaru, A.; Kerwin, B.; Chen, Y.; Ortiz, R. P.; Facchetti, A.; Marks, T. J. All-Polymer Solar Cells Incorporating Readily Accessible Naphthalene Diimide and Isoindigo

https://doi.org/10.1021/acs.jctc.4c00817
J. Chem. Theory Comput. 2024, 20, 10059−10070

Acceptor Polymers for Improved Light Harvesting. *Chem. Mater.* **2022**, *34* (7), 3267−3279.
(36) Ghosh, S.; Gueskine, V.; Berggren, M.; Zozoulenko, I. V. Electronic Structures and Optical Absorption of N-Type Conducting Polymers at Different Doping Levels. *J. Phys. Chem. C* **2019**, *123* (25), 15467−15476.
(37) Moia, D.; Giovannitti, A.; Szumska, A. A.; Maria, I. P.; Rezasoltani, E.; Sachs, M.; Schnurr, M.; Barnes, P. R. F.; McCulloch, I.; Nelson, J. Design and Evaluation of Conjugated Polymers with Polar Side Chains as Electrode Materials for Electrochemical Energy Storage in Aqueous Electrolytes. *Energy Environ. Sci.* **2019**, *12* (4), 1349−1357.
(38) Scholes, D. T.; Hawks, S. A.; Yee, P. Y.; Wu, H.; Lindemuth, J. R.; Tolbert, S. H.; Schwartz, B. J. Overcoming Film Quality Issues for Conjugated Polymers Doped with F_4TCNQ by Solution Sequential Processing: Hall Effect, Structural, and Optical Measurements. *J. Phys. Chem. Lett.* **2015**, *6* (23), 4786−4793.
(39) Scholes, D. T.; Yee, P. Y.; Lindemuth, J. R.; Kang, H.; Onorato, J.; Ghosh, R.; Luscombe, C. K.; Spano, F. C.; Tolbert, S. H.; Schwartz, B. J. The Effects of Crystallinity on Charge Transport and the Structure of Sequentially Processed F_4TCNQ-Doped Conjugated Polymer Films. *Adv. Funct. Mater.* **2017**, *27* (44), No. 1702654.
(40) Jacobs, I. E.; Aasen, E. W.; Oliveira, J. L.; Fonseca, T. N.; Roehling, J. D.; Li, J.; Zhang, G.; Augustine, M. P.; Mascal, M.; Moulé, A. J. Comparison of Solution-Mixed and Sequentially Processed P3HT:F4TCNQ Films: Effect of Doping-Induced Aggregation on Film Morphology. *J. Mater. Chem. C* **2016**, *4* (16), 3454−3466.
(41) Aguirre, J. C.; Hawks, S. A.; Ferreira, A. S.; Yee, P.; Subramaniyan, S.; Jenekhe, S. A.; Tolbert, S. H.; Schwartz, B. J. Sequential Processing for Organic Photovoltaics: Design Rules for Morphology Control by Tailored Semi-Orthogonal Solvent Blends. *Adv. Energy Mater.* **2015**, *5* (11), No. 1402020.
(42) Chew, A. R.; Ghosh, R.; Shang, Z.; Spano, F. C.; Salleo, A. Sequential Doping Reveals the Importance of Amorphous Chain Rigidity in Charge Transport of Semi-Crystalline Polymers. *J. Phys. Chem. Lett.* **2017**, *8* (20), 4974−4980.
(43) Frisch, M. J.; Trucks, G. W.; Schlegel, H. B.; Scuseria, G. E.; Robb, M. A.; Cheeseman, J. R.; Scalmani, G.; Barone, V.; Petersson, G. A.; Nakatsuji, H.; Li, X.; Caricato, M.; Marenich, A. V.; Bloino, J.; Janesko, B. G.; Gomperts, R.; Mennucci, B.; Hratchian, H. P.; Ortiz, J. V.; Izmaylov, A. F.; Sonnenberg, J. L.; Williams-Young, D.; Ding, F.; Lipparini, F.; Egidi, F.; Goings, J.; Peng, B.; Petrone, A.; Henderson, T.; Ranasinghe, D.; Zakrzewski, V. G.; Gao, J.; Rega, N.; Zheng, G.; Liang, W.; Hada, M.; Ehara, M.; Toyota, K.; Fukuda, R.; Hasegawa, J.; Ishida, M.; Nakajima, T.; Honda, Y.; Kitao, O.; Nakai, H.; Vreven, T.; Throssell, K.; Montgomery, J. A., Jr.; Peralta, J. E.; Ogliaro, F.; Bearpark, M. J.; Heyd, J. J.; Brothers, E. N.; Kudin, K. N.; Staroverov, V. N.; Keith, T. A.; Kobayashi, R.; Normand, J.; Raghavachari, K.; Rendell, A. P.; Burant, J. C.; Iyengar, S. S.; Tomasi, J.; Cossi, M.; Millam, J. M.; Klene, M.; Adamo, C.; Cammi, R.; Ochterski, J. W.; Martin, R. L.; Morokuma, K.; Farkas, O.; Foresman, J. B.; Fox, D. J. *Gaussian16*, Revision C.01; Gaussian Inc., 2016.
(44) Stanfield, D. A.; Mehmedović, Z.; Schwartz, B. J. Vibrational Stark Effect Mapping of Polaron Delocalization in Chemically Doped Conjugated Polymers. *Chem. Mater.* **2021**, *33* (21), 8489−8500.
(45) Wang, C.; Zhang, Z.; Pejić, S.; Li, R.; Fukuto, M.; Zhu, L.; Sauvé, G. High Dielectric Constant Semiconducting Poly(3-Alkylthiophene)s from Side Chain Modification with Polar Sulfinyl and Sulfonyl Groups. *Macromolecules* **2018**, *51* (22), 9368−9381.
(46) Warren, R.; Blom, P. W. M.; Koch, N. Molecular *p* -Doping Induced Dielectric Constant Increase of Polythiophene Films Determined by Impedance Spectroscopy. *Appl. Phys. Lett.* **2023**, *122* (15), No. 152108.
(47) Zayat, B.; Elizalde-Segovia, R.; Das, P.; Salamat, C. Z.; Irshad, A.; Tolbert, S. H.; Thompson, B. C.; Narayanan, S. R. The Role of Functionalized Conducting Polymer Binders in Improving Power Density and Cycle Life of Lithium-Sulfur Batteries. *J. Electrochem. Soc.* **2022**, *169* (10), No. 100515.
(48) Adamo, C.; Barone, V. Toward Reliable Density Functional Methods without Adjustable Parameters: The PBE0 Model. *J. Chem. Phys.* **1999**, *110* (13), 6158−6170.
(49) Henderson, T. M.; Izmaylov, A. F.; Scalmani, G.; Scuseria, G. E. Can Short-Range Hybrids Describe Long-Range-Dependent Properties? *J. Chem. Phys.* **2009**, *131* (4), No. 044108.
(50) Chai, J.-D.; Head-Gordon, M. Long-Range Corrected Hybrid Density Functionals with Damped Atom−Atom Dispersion Corrections. *Phys. Chem. Chem. Phys.* **2008**, *10* (44), 6615−6620.
(51) Luzanov, A. V.; Sukhorukov, A. A.; Umanskii, V. É. Application of Transition Density Matrix for Analysis of Excited States. *Theor. Exp. Chem.* **1976**, *10* (4), 354−361.
(52) Martin, R. L. Natural Transition Orbitals. *J. Chem. Phys.* **2003**, *118* (11), 4775−4777.
(53) Feng, R.; Yu, X.; Autschbach, J. Spin−Orbit Natural Transition Orbitals and Spin-Forbidden Transitions. *J. Chem. Theory Comput.* **2021**, *17* (12), 7531−7544.
(54) Casanova, D. Theoretical Modeling of Singlet Fission. *Chem. Rev.* **2018**, *118* (15), 7164−7207.
(55) Kimber, P.; Plasser, F. Toward an Understanding of Electronic Excitation Energies beyond the Molecular Orbital Picture. *Phys. Chem. Chem. Phys.* **2020**, *22* (11), 6058−6080.
(56) Sergentu, D.; Booth, C. H.; Autschbach, J. Probing Multiconfigurational States by Spectroscopy: The Cerium XAS L_3-edge Puzzle. *Chem. - Eur. J.* **2021**, *27* (25), 7239−7251.
(57) Humphrey, W.; Dalke, A.; Schulten, K. VMD: Visual Molecular Dynamics. *J. Mol. Graphics* **1996**, *14* (1), 33−38.
(58) Stanfield, D. A.; Wu, Y.; Tolbert, S. H.; Schwartz, B. J. Controlling the Formation of Charge Transfer Complexes in Chemically Doped Semiconducting Polymers. *Chem. Mater.* **2021**, *33* (7), 2343−2356.
(59) Wu, E. C.-K.; Salamat, C. Z.; Tolbert, S. H.; Schwartz, B. J. Molecular Dynamics Study of the Thermodynamics of Integer Charge Transfer vs Charge-Transfer Complex Formation in Doped Conjugated Polymers. *ACS Appl. Mater. Interfaces* **2022**, *14* (23), 26988−27001.
(60) Tozer, D. J. Relationship between Long-Range Charge-Transfer Excitation Energy Error and Integer Discontinuity in Kohn−Sham Theory. *J. Chem. Phys.* **2003**, *119* (24), 12697−12699.
(61) Dreuw, A.; Head-Gordon, M. Failure of Time-Dependent Density Functional Theory for Long-Range Charge-Transfer Excited States: The Zincbacteriochlorin−Bacteriochlorin and Bacteriochlorophyll−Spheroidene Complexes. *J. Am. Chem. Soc.* **2004**, *126* (12), 4007−4016.
(62) Maitra, N. T. Charge Transfer in Time-Dependent Density Functional Theory. *J. Phys.: Condens. Matter* **2017**, *29* (42), No. 423001.
(63) Kümmel, S. Charge-Transfer Excitations: A Challenge for Time-Dependent Density Functional Theory That Has Been Met. *Adv. Energy Mater.* **2017**, *7* (16), No. 1700440.
(64) Mester, D.; Kállay, M. Charge-Transfer Excitations within Density Functional Theory: How Accurate Are the Most Recommended Approaches? *J. Chem. Theory Comput.* **2022**, *18* (3), 1646−1662.
(65) Shao, Y.; Mei, Y.; Sundholm, D.; Kaila, V. R. I. Benchmarking the Performance of Time-Dependent Density Functional Theory Methods on Biochromophores. *J. Chem. Theory Comput.* **2020**, *16* (1), 587−600.
(66) Narsaria, A. K.; Ruijter, J. D.; Hamlin, T. A.; Ehlers, A. W.; Guerra, C. F.; Lammertsma, K.; Bickelhaupt, F. M. Performance of TDDFT Vertical Excitation Energies of Core-Substituted Naphthalene Diimides. *J. Comput. Chem.* **2020**, *41* (15), 1448−1455.
(67) Conradie, J.; Wamser, C. C.; Ghosh, A. Understanding Hyperporphyrin Spectra: TDDFT Calculations on Diprotonated Tetrakis(*p*-Aminophenyl)Porphyrin. *J. Phys. Chem. A* **2021**, *125* (46), 9953−9961.
(68) Wei, P.; Oh, J. H.; Dong, G.; Bao, Z. Use of a 1 *H* -Benzoimidazole Derivative as an *n*-Type Dopant and To Enable Air-Stable Solution-Processed *n*-Channel Organic Thin-Film Transistors. *J. Am. Chem. Soc.* **2010**, *132* (26), 8852−8853.

https://doi.org/10.1021/acs.jctc.4c00817
J. Chem. Theory Comput. 2024, 20, 10059−10070